

Temperature of Solar Prominences Obtained with the Fast Imaging Solar Spectrograph on the 1.6 m New Solar Telescope at the Big Bear Solar Observatory

Hyungmin Park · Jongchul Chae · Donguk Song · Ram Ajour Maurya · Heesu Yang · Young-Deuk Park · Bi-Ho Jang · Jakyoungh Nah · Kyung-Suk Cho · Yeon-Han Kim · Kwangsu Ahn · Wenda Cao · Philip R. Goode

Received: 2 July 2012 / Accepted: 6 March 2013 / Published online: 29 March 2013
© Springer Science+Business Media Dordrecht 2013

Abstract We observed solar prominences with the Fast Imaging Solar Spectrograph (FISS) at the Big Bear Solar Observatory on 30 June 2010 and 15 August 2011. To determine the temperature of the prominence material, we applied a nonlinear least-squares fitting of the radiative transfer model. From the Doppler broadening of the H α and Ca II lines, we determined the temperature and nonthermal velocity separately. The ranges of temperature and nonthermal velocity were 4000–20 000 K and 4–11 km s⁻¹. We also found that the temperature varied much from point to point within one prominence.

Keywords Chromosphere, quiet · Heating, chromospheric · Prominences, quiescent · Spectral line, broadening

1. Introduction

A proper understanding of the nature of solar prominences relies on precise measurements of their basic physical parameters: temperature, density, mass motion, and magnetic field. Temperature is of particular interest in this study. It is well known that the temperature of the prominence material is about 10⁴ K, whereas the corona has a temperature of 10⁶ K. Precise measurements of the temperature in a prominence are needed to estimate the other physical parameters. For example, hydrogen is partially ionized in the prominence so that

Initial Results from FISS
Guest Editor: Jongchul Chae

H. Park (✉) · J. Chae · D. Song · R.A. Maurya · H. Yang
Astronomy Program, Department of Physics and Astronomy, Seoul National University, Seoul,
Republic of Korea
e-mail: hmpark@astro.snu.ac.kr

Y.-D. Park · B.-H. Jang · J. Nah · K.-S. Cho · Y.-H. Kim
Korea Astronomy and Space Science Institute, Daejeon, Republic of Korea

K. Ahn · W. Cao · P.R. Goode
Big Bear Solar Observatory, New Jersey Institute of Technology, Big Bear City, CA, USA

the degree of ionization may be sensitive to the temperature. In addition, the density can only be determined if the temperature is known.

The most common way to determine the prominence temperature is to use the absorption width of a spectral line. The major broadening in the line is the Doppler broadening, which contains the thermal as well as the nonthermal contribution. If the value of the nonthermal contribution is known, one can obtain the thermal contribution from the line broadening. In some studies, the nonthermal contribution was neglected so that the obtained temperatures represented the upper limit to the real value (Ellison, 1952; Jefferies, 1955; Mein and Mein, 1991). In other studies, more than one line was used, and both the thermal and nonthermal contributions were determined independently (Hirayama, 1963, 1971; Jefferies, 1956, 1962; Gallegos and Machado, 1973; Nikolsky, Gulyaev, and Nikolskaya, 1971; Landman, Edberg, and Laney, 1977; Zhang *et al.*, 1987; Li *et al.*, 1998; Mein and Mein, 1991; Stellmacher, Wiehr, and Dammasch, 2003).

Temperatures obtained through the line width method have a wide range from 4000 K to 20 000 K. How can we understand these results? The temperature probably depends on the individual prominences observed. Another possible explanation is that it depends on the spectral lines used. For instance, Hirayama (1963) obtained a prominence temperature of 4000 K from helium and metallic lines, and Jefferies (1956) obtained 20 000 K by combining the H α line with the helium D3 line. It is not surprising that the measured temperatures depend on the line used. The visibility of a line from a specific atom is determined by the ionization and excitation process in the prominence, which depends on the temperature. Therefore, each detected line may have its own range of temperature. Finally, some of the previous studies indicated that the temperature varies with the position and time inside each prominence. To understand the wide range of the reported temperatures of the prominences, more observations are needed, especially using spectrographs with space- and time-resolving capabilities.

The Fast Imaging Solar Spectrograph (FISS) is one of the instruments of the 1.6 m New Solar Telescope (NST) at the Big Bear Solar Observatory. It is an imaging spectrograph designed to produce data with high spectral, spatial, and temporal resolutions that are suited for the study of fine-scaled structures and dynamics in the solar chromosphere (Chae *et al.*, 2012). The FISS has the capability of recording two spectral bands simultaneously and performing imaging based on the linear motion of a two-mirror scanner. From the H α and the Ca II 8542 band, one can measure the temperature and nonthermal velocity in chromospheric features such as filaments (prominences), quiet regions, and active regions. In addition, the imaging capability of the FISS enables us to study the dynamics of such features. These capabilities can also be exploited for observations of solar prominences. So far, researchers have mostly observed only a limited part of a prominence with a spectrograph; our observations of prominences with the FISS will provide detailed knowledge on the variation with position of the physical quantities within individual prominences.

We here describe prominence observations using the FISS with our data reduction and spectral analysis, and the results on the temperatures of solar prominences. For the spectral analysis, we employed a simple model of radiative transfer that takes into account the effect of finite optical depth.

2. Data and Analysis

2.1. Observation

The observations were performed with the FISS on the 1.6 m New Solar Telescope (NST) at the Big Bear Solar Observatory (BBSO). This instrument is a high-dispersion Echelle spec-

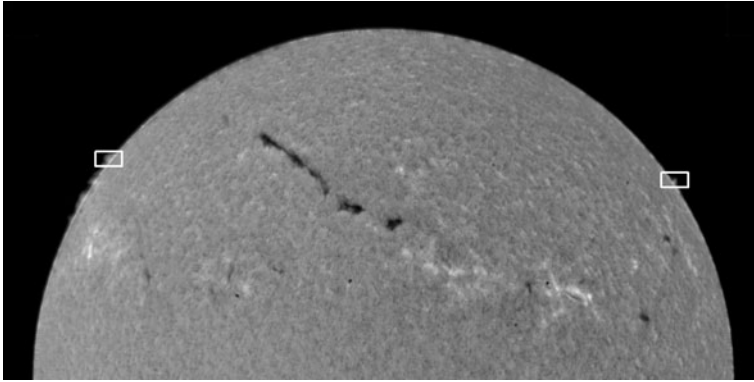


Figure 1 $H\alpha$ image obtained on 30 June 2010 at the BBSO. The two rectangles represent the prominences on the east and west limb observed by the FISS. The field-of-view is $72'' \times 40''$.

trograph of near-Littrow type, with a $32 \mu\text{m}$ slit width ($0.16''$), a focal length of 1.5 m, a focal ratio of F/26, and high spectral orders: 34th at $H\alpha$ and 26th at $\text{Ca II } 8542 \text{ \AA}$. It is currently the largest operating solar telescope in the world with Echelle grating and fast CCD, and we obtained data with high spatial, spectral, and time resolutions. More information about the FISS performance can be found in Chae *et al.* (2012).

On 30 June 2010, we observed one prominence on the east limb and another on the west limb (Figure 1). The two rectangles in the figure show the two fields of view of the observations. The exposure time was 90 ms, and the scanning time was 140 s. In addition, we observed a prominence in the east limb on 15 August 2011. In contrast to 30 October 2010, the adaptive optics (AO) system worked on this day, and the prominence was scanned stably with little image motion along the slit direction. In this observation, the exposure was 30 ms, and the scanning time was 40 s. The observed spectra were treated with basic processes such as dark-subtraction and flat-fielding. The processed data were compressed and stored based on the principal component analysis (PCA). This PCA compression reduces noise as well as the data size without much loss of information (Chae *et al.*, 2012). In addition, the aureole light spectra on the $H\alpha$ and Ca II lines were removed carefully by subtracting the spectra from outside the prominence. The two spectral bands were spatially aligned by shifting the Ca II spectra by a fixed amount with respect to the $H\alpha$ spectra.

2.2. Spectral Analysis

The equation for radiative transfer across a layer is well known. The equation consists of background radiation and the contribution of the source from the object itself. In the case of limb prominences, background radiation can be ignored. If the source function is constant along the line of sight, the intensity is theoretically modeled with the equation using optical thickness τ

$$I = S(1 - e^{-\tau}), \quad (1)$$

where S is the source function.

In prominences/filaments, thermal broadening is much more significant in the formation of spectral lines than collisional broadening, so that the optical thickness profile may be written in the Gaussian functional form

$$\tau = \tau_0 \exp \left[- \left(\frac{\lambda - \lambda_c}{\Delta \lambda_D} \right)^2 \right], \quad (2)$$

where $\Delta\lambda_D$ is the Doppler width, τ_0 is the optical thickness at line center, and λ_c is the central wavelength of the absorption profile, which is a measure of the Doppler shift.

It is well known that Doppler broadening contains a thermal and a nonthermal contribution. If we also assume that the temperature is constant along the line of sight and the velocity distribution of the nonthermal motion is Gaussian as well, the Doppler width in Equation (2) is expressed by

$$\Delta\lambda_D = \frac{\lambda}{c} \sqrt{\frac{2kT}{M} + \xi^2}, \quad (3)$$

where λ is the wavelength at rest, T is the mean kinetic temperature along the line of sight, M is the mass of the atom, and ξ is the nonthermal velocity (Tandberg-Hanssen, 1995; Labrosse *et al.*, 2010). The nonthermal velocity ξ incorporates all kinds of unresolved motion along the line of sight, including random motions of fine-structure threads as investigated by Gunár *et al.* (2012). We determined the values of these parameters with a least-squares fitting.

We applied the radiative transfer model to the spectra of the H α and Ca II 8542 Å lines. Three methods were tested to estimate the temperature of these prominences. First, we applied the model to each line separately and obtained two Doppler-broadening values ($\Delta\lambda_{D,H\alpha}$, $\Delta\lambda_{D,Ca}$). Second, we regarded the temperature and nonthermal velocity as independent parameters and fitted the two line profiles together. Finally, we adopted the second approach above, but reduced the number of free parameters by introducing the line-of-sight velocity as an independent variable instead of the center positions of the two lines. This reduction is based on the assumption that the two lines are formed in the same volume.

We found that the results are almost the same and depend very little on the chosen method. We decided to choose the first method to determine the prominence temperatures since it is commonly used, can be applied to each line separately, and needs fewer assumptions.

In the analysis, it is not necessary to take into account the instrumental broadening. Using a HeNe (632.8 nm) laser, Chae *et al.* (2012) estimated the instrumental broadening as 1.6 pm, which corresponds to about 2.0 pm at the wavelengths of H α and Ca II 8542 Å, which is so small that it is negligible.

3. Results

Figure 2 indicates how a prominence on the limb appears at the centers of the H α (top row) and Ca II (bottom row) lines without AO. The prominence appears to be much darker than the disk in the Ca II line, while its brightness is comparable to the disk value in the H α line. We found that the intensity gradually decreases from the disk to the prominence in the H α line, but sharply drops in the Ca II line. Despite this difference, the H α and Ca II images of the prominence look similar. There are some differences in the morphology between these lines, which may not be physically fundamental, but seem to reflect mostly the difference in optical thickness, which will be described below. From the H α and Ca II spectra, we found that the Ca II line width is smaller than the H α line width. Moreover, the solar limb appears to be irregular, which is due to the image motion from atmospheric disturbances. Since a prominence is fainter than the disk and not visible in molecular bands such as TiO and G bands, it will be hard to observe the prominence with the AO properly operating. If a prominence happens to lie near a sunspot as it did on 15 August 2011, it is possible to obtain the data with better quality because the AO can operate.

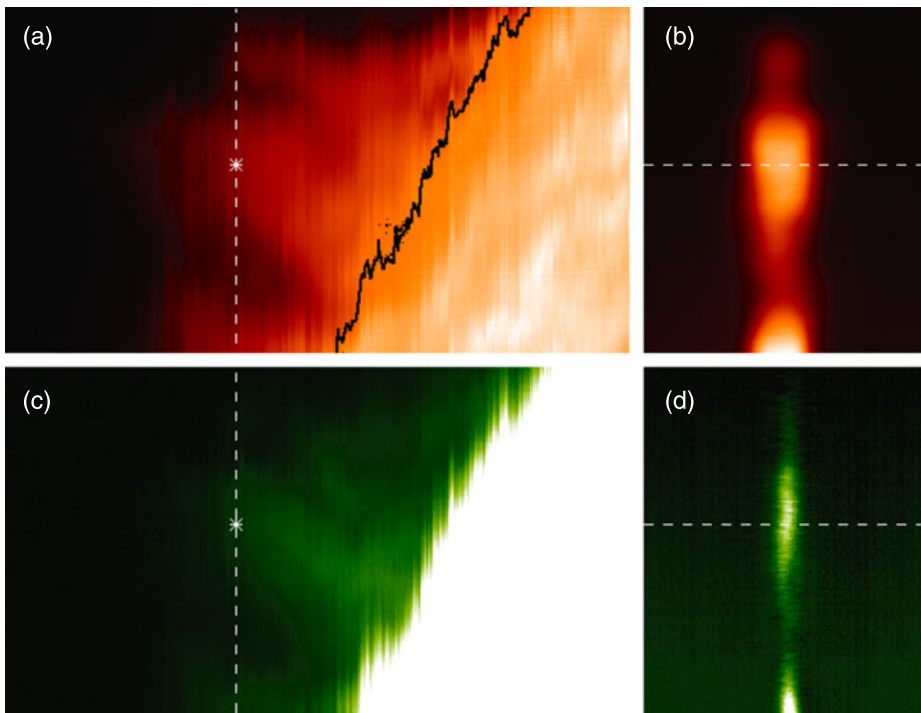


Figure 2 Scan images (left column) and spectrograms (right column) of the prominence on the east limb observed in H α (top row) and Ca II 8542 Å (bottom row) on 30 June 2010. A black curve in the upper left image marks the boundary of the solar disk in Ca II as shown in the lower left image. Vertical dashed lines in the left-hand-side panels represent the slit position along which the spectrograms in the right-hand-side panels were taken. Horizontal dashed lines in the right-hand-side panels correspond to the positions indicated by asterisks in the left-hand-side panels. Line profiles along the horizontal dashed lines are shown in Figure 3.

To illustrate the spectral properties of the prominence in the H α and Ca II lines, we selected an arbitrary position (marked by *) as indicated in Figure 2. Figure 3 shows the line profiles and fitting results in the H α and Ca II lines. The H α line was fitted with $\tau_0 = 3.43$, $\Delta\lambda_0 = 0.034$ nm, and $V_D = -1.15$ km s $^{-1}$. The Ca II line was fitted with $\tau_0 = 0.29$, $\Delta\lambda_0 = 0.023$ nm, and $V_D = -2.12$ km s $^{-1}$. The H α line profile has a higher peak value than the Ca II line profile. Furthermore, the signal-to-noise ratio in the H α line profile is higher than that of the Ca II. Despite this difference, both lines are fairly well fitted. From the model fitting, we found that the prominence is optically thick in the H α line, but optically thin in the Ca II line. In an optically thin case, optical thickness and source function cannot be separately determined; therefore, their values should be taken carefully. The Doppler velocity in the H α line is found to be close to the Ca II line, which supports our assumption that the two lines are formed in the same volume of the prominence. As a result, the temperature and the nonthermal velocity are estimated to be about 11 000 K and 7.8 km s $^{-1}$. These values are not far from previously reported values.

The left panel of Figure 4 presents the scatter plot of the Doppler width ($\Delta\lambda_{D,H\alpha}$) versus the Doppler width ($\Delta\lambda_{D,Ca}$) for the east-limb prominence of 30 June 2010. The Doppler widths are in the range of 0.028–0.037 nm in the H α line and 0.012–0.031 nm for the Ca II line. The correlation coefficient (C) between the line width is 0.61. Blue and red curves, obtained from Equation (3), represent the iso- T and iso- ξ curves, respectively. From these

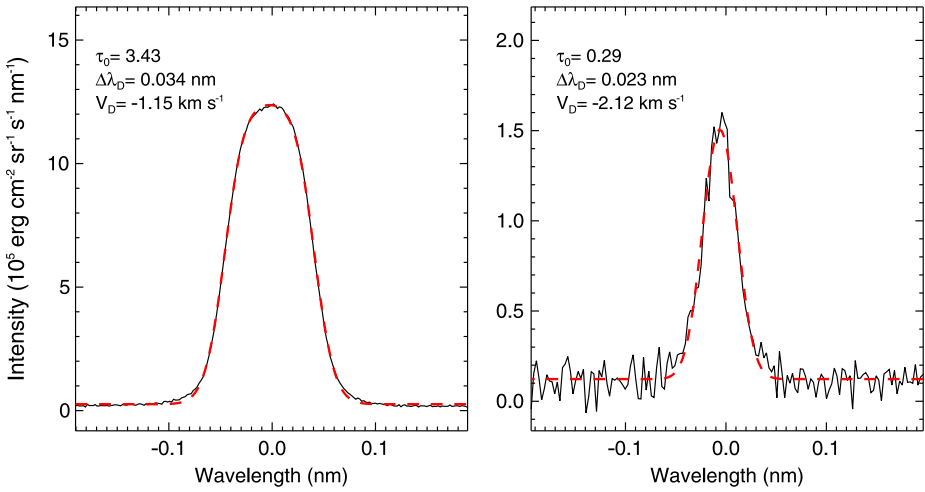


Figure 3 Line profile and fitting result for H α (left) and Ca II (right). These two profiles come from the position of the asterisk symbols in Figure 2. Solid (black) and dashed (red) lines are the line profiles and the fitting result from our analysis.

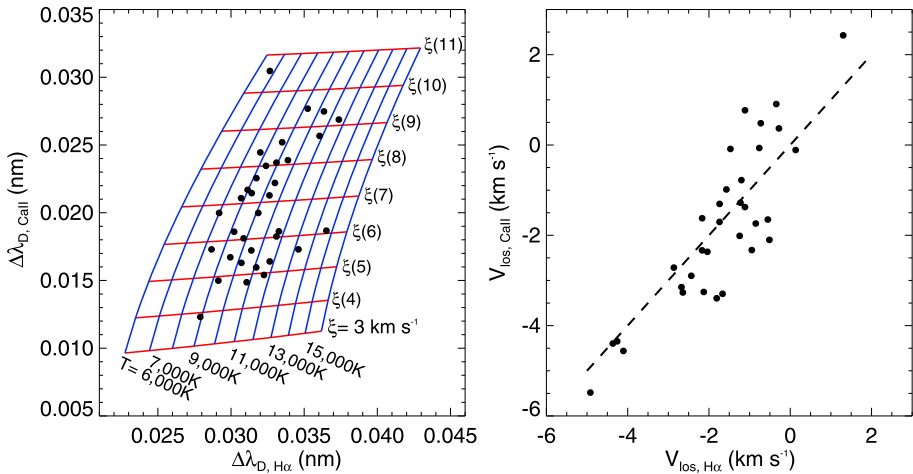


Figure 4 Scatter plots between $\Delta\lambda_{D,H\alpha}$ and $\Delta\lambda_{D,Ca}$ (left panel), and between $V_{los,H\alpha}$ and $V_{los,Ca}$ (right panel) for the east-limb prominence on 30 June 2010. In the left-hand-side panel, the blue and red curves represent iso-temperature and iso-nonthermal velocity curves. In the right-hand-side panel, the dashed line represents the same Doppler velocities in both lines.

curves, we can estimate the temperature and nonthermal velocity for each measurement marked by a dot. We found that T ranges from 7000 K to 14 000 K, and ξ ranges from 4 km s⁻¹ to 11 km s⁻¹. The most probable values for the temperature and nonthermal velocity are estimated to be $10\,200 \pm 1580$ K and 6.9 ± 1.6 km s⁻¹.

The right panel shows the scatter plot between the Doppler velocity $V_{los,H\alpha}$ and $V_{los,Ca}$. If the H α and Ca II lines are formed in the same volume, the Doppler velocities derived from the two lines are expected to coincide, which leads to the theoretical relationship indicated

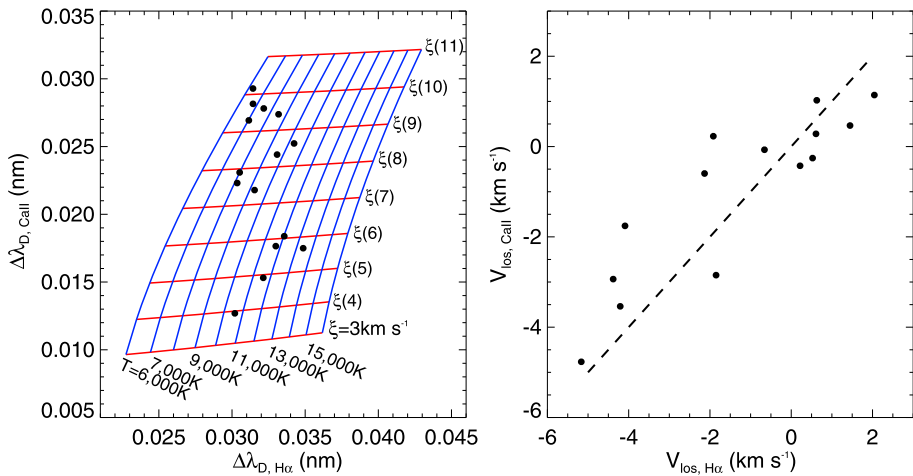


Figure 5 The same as Figure 4, but for the west-limb prominence observed on 30 June 2010.

by the dashed line (right panel). We find from the plot that the measured Doppler velocities do not deviate much from the theoretical values. The standard deviation from this line is 0.9 km s^{-1} , which we consider to be tolerable.

Figure 5 presents the results from the west-limb prominence of 30 June 2010. Since this prominence is smaller and fainter than the eastern one, there are fewer data points. The measured ranges of temperature of $6000 \text{ K} < T < 14000 \text{ K}$ and the nonthermal velocity of $4 \text{ km s}^{-1} < \xi < 10 \text{ km s}^{-1}$ are not much different from the east-limb prominence. The correlation coefficient between the line width is $C = -0.05$. The most probable values for the temperature and nonthermal velocity are estimated to be $T = 9390 \pm 2170 \text{ K}$ and $\xi = 7.6 \pm 1.9 \text{ km s}^{-1}$. The standard deviation (right panel) of the difference between the measure and theoretical values of the nonthermal velocity is found to be 1.17 km s^{-1} , which is a little higher than the above value, but still is fairly acceptable.

Figure 6 shows the scatter plot of the same parameters for the prominence on 15 August 2011. Doppler widths for the H α and Ca II lines are found in the ranges $0.025\text{--}0.031 \text{ nm}$ and $0.01\text{--}0.021 \text{ nm}$, respectively. The correlation coefficient between the line width is $C = 0.63$. The most probable values for the temperature and nonthermal velocity are estimated to be $T = 8680 \pm 1070 \text{ K}$ and $\xi = 4.6 \pm 0.9 \text{ km s}^{-1}$. In addition, the standard deviation of the Doppler velocities from the theoretical values is estimated to be 0.38 km s^{-1} . The Doppler widths and standard deviation for the prominence on 15 August 2011 are smaller compared to the two prominences on 30 June 2010. We can explain these differences in terms of the operation of the adaptive optics (AO) system, short exposure time, or the characteristics of individual prominences. A better operation of the AO and a short exposure enable us to obtain data with higher spatial and temporal resolutions. The operation of the AO corrects for atmospheric distortion, which allows us to obtain data with higher spatial resolution and smaller errors in data alignment. The short exposure may also be useful in freezing the seeing. On the other hand, a short exposure may also bring about another effect of obscuring faint parts, with bias given to bright parts. Alternatively, the difference between this prominence and the other prominences might be due to intrinsic variations from prominence to prominence.

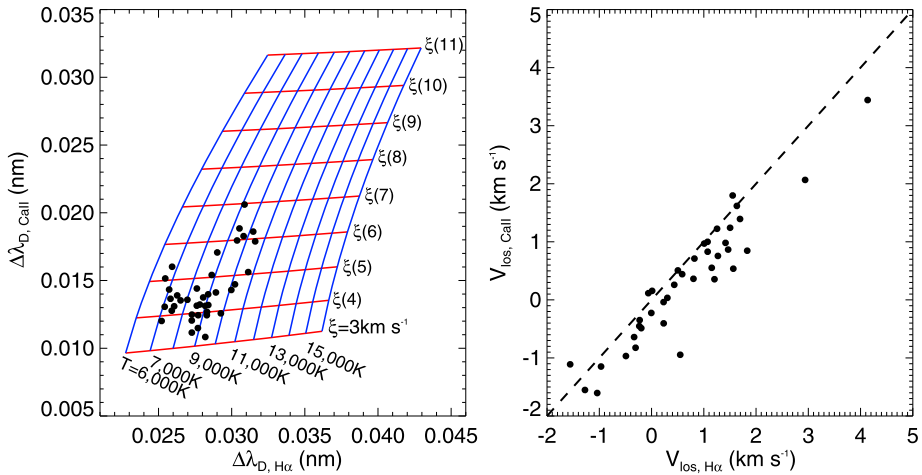


Figure 6 The same as Figure 4, but for the west-limb prominence on 15 August 2011.

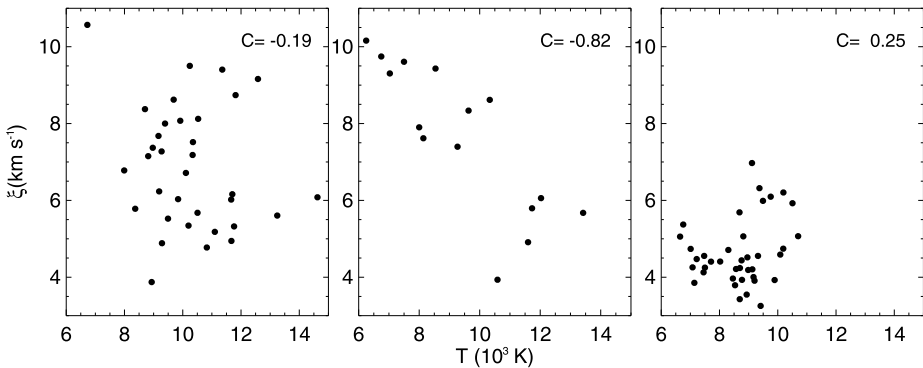


Figure 7 Scatter plots of T versus ξ of the east-limb prominence of 30 June 2010 (left), the west-limb prominence of 30 June 2010 (middle), and the east-limb prominence of 15 August 2011 (right). The correlation coefficient between T and ξ of the prominences is shown in each panel.

Figure 7 is presented to investigate the correlation between the temperature and nonthermal velocity in the three prominences. The left (east-limb prominence of 30 June 2010) and the right (east-limb prominence of 15 August 2011) panels show that the temperature and nonthermal velocity are not correlated ($C = -0.19$ and $C = 0.25$, respectively). In the middle panel (west-limb prominence of 30 June 2010), a negative correlation ($C = -0.82$) exists between the temperature and nonthermal velocity. Since the prominence is small and the data quality is poorer than that of the other data, it is hard to accept this result. We have checked whether the model fitting is appropriate for the prominence data and whether we can trust our results or not. We conclude that this correlation is due to the relationship between the temperature and nonthermal velocity as indicated by Equation (3). If the broadening is constant and the temperature is high, the nonthermal velocity should have a low velocity, and vice versa. These values may affect the results shown in the middle panel of Figure 7.

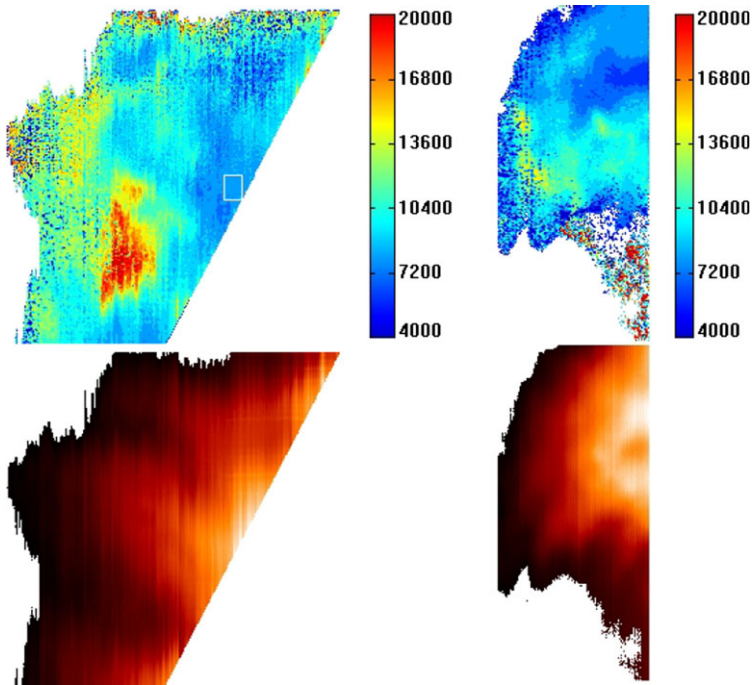


Figure 8 The temperature (top row) and intensity maps (bottom row) of the prominences observed on 30 June 2010 (left column) and on 15 August 2011 (right column). A white square marked in the upper left corner represents the region where the random error in the temperature measurement is estimated. The temperature maps are derived from the model fitting, the intensity maps from the integrated intensities.

Figure 8 presents maps of the temperature and integrated intensity of the two selected prominences of 30 June 2010 (left column) and 15 August 2011 (right column). The temperature ranges from about 4000 K to about 20 000 K in the two prominences. Obviously, the temperature varies from region to region within the same prominence. A particular example is the region with the highest temperature ($T \approx 20\,000$ K) seen in the prominence of 30 June 2010. Interestingly, this region corresponds to a fainter part of the prominence. Excluding this feature, we see a tendency that the temperature increases outward in the prominence. This kind of spatial variation was previously reported by Hirayama (1971). Conversely, this tendency is not obvious in the other prominence observed on 15 August 2011. The temperature in the boundary is comparable to the central part of the prominence. This is somewhat different from the conventional expectation that the outer part will have a higher temperature because it is in contact with the hot corona (the so-called prominence-corona transition region – PCTR). We failed in finding any indication of a temperature increase at the fainter outer parts. Currently, we have no reasonable explanation for this peculiar behavior. This prominence appears to be consistent with the result of Zhang *et al.* (1987) and Mouradian and Leroy (1977) in that there is no regular increase in temperature from the center to the edge in a prominence. As a result, our study presents examples of both patterns.

We measured the random error in the temperature of the prominence. As marked in Figure 8, we selected a region with an apparently uniform temperature and determined the standard deviation in the region of interest as a measurement of random error in the tem-

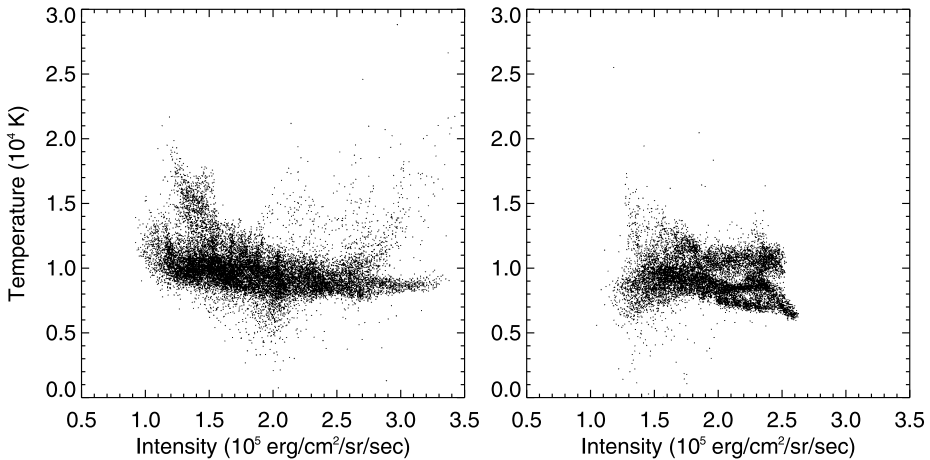


Figure 9 Scatter plots of T versus I (integrated intensity over the line) for two selected prominences on 30 June 2010 (left panel) and on 15 August 2011 (right panel). The estimated temperatures and correlation coefficients of the prominences are 10600 ± 2440 K and 9450 ± 2000 K, and -0.31 and -0.15 , respectively.

perature. The error was estimated to be less than 300 K. Compared with the temperature we obtained, the error is small and tolerable.

Figure 9 presents the scatter plots between the integrated intensity over the line and the temperature of the two prominences observed on 30 June 2010 (left panel) and 15 August 2011 (right panel). It shows that the temperatures in the prominences are centered around 10 000 K. The prominence temperature decreases with the intensity, and the correlation coefficients between their temperatures and intensities are determined to be -0.31 and -0.15 , respectively. We found a similar pattern in that the spread in the temperature is smaller within the pixels of higher intensities than within the pixels of lower intensities. This tendency may be real because the spreads are much larger than the estimated measurement errors.

Our analysis has taken into account the effects of finite optical thickness. If the optical thickness is larger than unity, the core will saturate to a constant value so that the line profile appears to be more broadened. Unless this effect is properly taken into account, the Doppler width will be overestimated, and hence the temperature. Our analysis is free from this problem since the optical thickness was treated as an independent parameter. Figure 10 shows the results of the fitting to the $H\alpha$ line profiles at two different positions in the prominence. The fitting in the left panel yields 3.5 as the estimate for the optical thickness. If the optical thickness is set to either a lower or higher value, the fitting becomes poorer, as can be seen from the figure (red and green dashed curves). This supports the validity of our treatment for the effect of finite optical thickness. The right panel, however, provides an example of a case where our analysis is not satisfactory. The line profile in this case shows a central reversal in the core, which may be due to self-absorption arising when the optical thickness is very large. The failure of our analysis in this case comes from the assumption that the source function is constant along the line of sight. This is a limitation of the model. Nevertheless, there are so few data points showing the central reversal in the $H\alpha$ line that this limitation does not significantly affect the statistics of the temperature measurements.

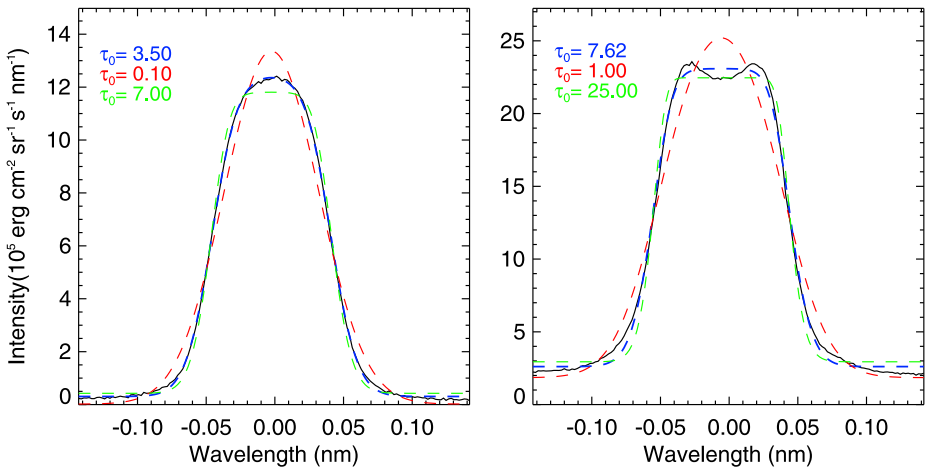


Figure 10 H α line profiles and fitting results with different τ_0 values at two different positions on the prominence of 30 June 2010. The black lines represent H α line profiles. The blue dashed curve represents the fitted profile with optical thickness τ_0 while the red dashed and green dashed curves represent the variation in the fitted profiles due to small/large values in the optical thickness from the fitted τ_0 over the H α line.

4. Discussion

In three prominences we determined the temperature of H α -emitting plasma based on the simultaneous measurements of the Doppler widths of the emission profile in the H α and Ca II 8542 Å lines. Our study showed that the temperature within each prominence varies from 4000 to 20 000 K and the nonthermal velocity varies from 4 to 11 km s⁻¹. The temperature has no correlation with the nonthermal velocity, but has a weak negative correlation with the brightness.

The estimated temperature range in the prominences is broad enough to be consistent with previous reports. According to Hirayama (1985), the reported temperature ranges from 4000 to 20 000 K. In addition, he suggested that the representative temperature can be set to 7000 K if only one value has to be chosen. Indeed, most researchers found that the temperatures are lower than 10 000 K (Stellmacher, Wiehr, and Dammasch, 2003; Mein and Mein, 1991; Landman, Edberg, and Laney, 1977; Li *et al.*, 1998; Hirayama, 1971). Some researchers, however, obtained temperatures in the higher range of 10 000–20 000 K (Ellison, 1952; Jefferies, 1955, 1956). We obtained not only temperatures as low as 4000 K, but also those as high as 20 000 K, including both of the ranges above.

We expect that the temperature might vary along the line of sight. It is well known that a prominence consists of several fine-scale structures (threads). That is, each of the threads has its own temperature, and the temperature we obtained might be the result of the average of several temperatures. For instance, in the multi-thread model of Gunár *et al.* (2008), which fits the UV observations quite well, even identical threads do produce T -variations along the line of sight just because of the random positioning of individual threads. If this is the case, we expect that the intrinsic temperature variation on the plane of the sky may be higher than the variation we observed.

Is the measured peak temperature of 20 000 K real? One might suspect that this is an artifact resulting from large Doppler widths that in fact should be attributed to the superposition of multi-velocity components along the line of sight. Assuming that a resulting

high temperature of, for instance, 20 000 K is due to two velocity threads with different line-of-sight velocities, but with the same temperature of 8000 K and the same nonthermal velocity of 6 km s^{-1} , what would the relative velocity between the two threads be? From the two-component fitting of the H α line, the relative line-of-sight velocity between the two components is about 25 km s^{-1} . This velocity corresponds to a Doppler shift of 0.7 \AA in the Ca II line, which should manifest itself in the two separated components of the spectral line. We observed that the profile of the Ca II line, however, shows only one component with moderate width. This inconsistency indicates that the hypothesis above is wrong, and strongly suggests that the measured high temperatures are real.

We plan to investigate the fine scale structures and temporal changes in the temperature in the prominences in more detail. Higher spatial resolution observations will be available when the next generation of adaptive optics is introduced to the NST. Based on time sequences of high-cadence observations, we will be able to examine the temporal variation in the temperatures of the prominences.

Acknowledgements This work was supported by the National Research Foundation of Korea (KRF-2008-220-C00022) and by the Development of Korean Space Weather Center, a project of KASI.

References

- Chae, J., Park, H.-M., Ahn, K., Yang, H., Park, Y.-D., Nah, J., Jang, B.H., Cho, K.-S., Cao, W., Goode, P.R.: 2012, *Solar Phys.* doi:[10.1007/s11207-012-0147-x](https://doi.org/10.1007/s11207-012-0147-x).
- Ellison, M.A.: 1952, *Mon. Not. Roy. Astron. Soc.* **112**, 679.
- Gallegos, H.G., Machado, M.E.: 1973, *Solar Phys.* **31**, 427.
- Gunár, S., Heinzel, P., Anzer, U., Schmieder, B.: 2008, *Astron. Astrophys.* **490**, 307.
- Gunár, S., Mein, P., Schmieder, B., Heinzel, P., Mein, N.: 2012, *Astron. Astrophys.* **543**, A93.
- Hirayama, T.: 1963, *Publ. Astron. Soc. Japan* **15**, 122.
- Hirayama, T.: 1971, *Solar Phys.* **17**, 50.
- Hirayama, T.: 1985, *Solar Phys.* **100**, 415.
- Jefferies, J.T.: 1955, *Mon. Not. Roy. Astron. Soc.* **115**, 617.
- Jefferies, J.T.: 1956, *Mon. Not. Roy. Astron. Soc.* **116**, 629.
- Jefferies, J.T., Orrall, F.Q.: 1962, *Astrophys. J.* **135**, 109.
- Labrosse, N., Heinzel, P., Vial, J.-C., Kucera, T., Parenti, S., Gunár, S., Schmieder, B., Kilper, G.: 2010, *Space Sci. Rev.* **151**, 243.
- Landman, D.A., Edberg, S.J., Laney, C.D.: 1977, *Astrophys. J.* **218**, 888.
- Li, K., Schmieder, B., Malherbe, J.-M., Roudier, T., Wiik, J.-E.: 1998, *Solar Phys.* **183**, 323.
- Mein, P., Mein, N.: 1991, *Solar Phys.* **136**, 317.
- Mouradian, Z., Leroy, J.L.: 1977, *Solar Phys.* **51**, 103.
- Nikolsky, G.M., Gulyaev, R.A., Nikolskaya, K.I.: 1971, *Solar Phys.* **21**, 332.
- Stellmacher, G., Wiehr, E., Dammasch, I.E.: 2003, *Solar Phys.* **217**, 133.
- Tandberg-Hanssen, E. 1995, *The Nature of Solar Prominences*, Kluwer Academic Publishers, Dordrecht, 199.
- Zhang, Q.Z., Hu, J., Fang, C., Livingston, W.C.: 1987, *Solar Phys.* **114**, 245.